Journal of Structural Biology 213 (2021) 107695

Contents lists available at ScienceDirect

Journal of Structural Biology

journal homepage: www.elsevier.com/locate/yjsbi

Algorithmic robustness to preferred orientations in single particle analysis by CryoEM

C.O.S. Sorzano [a,*], D. Semchonok [b], S.-C. Lin [c], Y.-C. Lo [d], J.L. Vilas [e], A. Jiménez-Moreno [a], M. Gragera [a], S. Vacca [f], D. Maluenda [a], M. Martínez [a], E. Ramírez-Aportela [a], R. Melero [a], A. Cuervo [a], J.J. Conesa [a], P. Conesa [a], P. Losana [a], L. del Caño [a], J. Jiménez de la Morena [a], Y. C. Fonseca [a], R. Sánchez-García [a], D. Strelak [a], E. Fernández-Giménez [a], F. de Isidro [a], D. Herreros [a], P.L. Kastritis [a], R. Marabini [g], B.D. Bruce [h], J.M. Carazo [a]

[a] Biocomputing Unit, Centro Nacional de Biotecnologia (CNB-CSIC), Darwin, 3, Campus Universidad Autonoma, 28049 Cantoblanco, Madrid, Spain
[b] ZIK HALOMEM & Institute of Biochemistry and Biotechnology, Martin Luther University Halle-Wittenberg, Biozentrum, Halle (Saale), Germany
[c] Genomics Research Center, Academia Sinica, Taipei 11529, Taiwan
[d] Dept. Biotechnology and Bioindustry Sciences, College of Bioscience and Biotechnology, National Cheng Kung University, Tainan 70101, Taiwan
[e] Dept. of Biomedical Engineering, Yale University, New Haven, United States
[f] Dept. of Biochemistry, Univ. Zurich, Winterthurerstr. 190, CH-8057 Zurich, Switzerland
[g] Escuela Politecnica Superior, Universidad Autónoma de Madrid, 28049 Cantoblanco, Madrid, Spain
[h] Dept. Biochemistry & Cellular and Molecular Biology, Univ. Tennessee Knoxville, Knoxville, TN 37996, United States

ARTICLE INFO

Keywords:
Electron microscopy
Single particle analysis
Preferred orientations

ABSTRACT

The presence of preferred orientations in single particle analysis (SPA) by cryo-Electron Microscopy (cryoEM) is currently one of the hurdles preventing many structural analyses from yielding high-resolution structures. Although the existence of preferred orientations is mostly related to the grid preparation, in this technical note, we show that some image processing algorithms used for angular assignment and three-dimensional (3D) reconstruction are more robust than others to these detrimental conditions. We exemplify this argument with three different data sets in which the presence of preferred orientations hindered achieving a 3D reconstruction without artifacts or, even worse, a 3D reconstruction could never be achieved.

1. Introduction

The existence of preferred orientations has been known for long as a factor inducing 3D artifacts in the maps of macromolecular structures studied by EM (Boisset et al., 1998). The problem is not so much the lack of information, which should obviously result in artifacts along the missing directions (Turonova et al., 2016) and anisotropic resolutions (Penczek, 2002; Unser et al., 2005), but the overabundance of some projection directions. This overabundance seems to be related to preferred interactions between the macromolecule and the air-water or support-water interface (Russo et al., 2014; Noble et al., 2018; Noble et al., 2018; Wei et al., 2018) and the time between grid preparation and freezing, which gives more or fewer opportunities to a single molecule to reach those interfaces (D'Imprima et al., 2019). From the data analysis point of view, overabundance should result in a better resolution perpendicular to the overabundant direction, but apart from that, it should not further interfere with the reconstruction process. In contrast with this last assumption, in many occasions, experimentalists have problems with angular distributions that have significantly large empty regions in the projection sphere (Naydenova and Russo, 2017). In some cases, it has been reported the same dataset processed with two different algorithms (Relion 3D autorefine and Xmipp highres) and one of them (Relion) having an angular distribution with missing regions (see Fig. 2 of Sorzano et al. (2018)). With real data one can never know what is the true underlying angular distribution, but for all methods based on a measure of the squared distance between a reference and an experimental image (and Relion and CryoSPARC are examples of this) we reported the existence of the "attraction" problem (see the mathematical proof in Eq. 6 in Sorzano et al. (2010)). This problem states that when a reference image (in Sorzano et al. (2010) they were 2D classes, but the

* Corresponding author.
E-mail address: carazo@cnb.csic.es (C.O.S. Sorzano).

https://doi.org/10.1016/j.jsb.2020.107695
Received 14 July 2020; Received in revised form 18 December 2020; Accepted 24 December 2020
Available online 7 January 2021

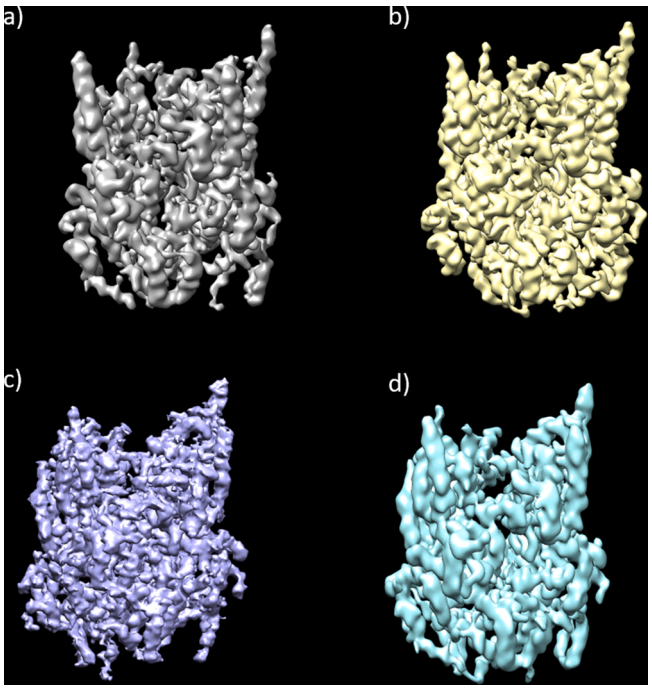

Fig. 2. Reconstruction of a modified version of the myddosome by CryoSPARC non-uniform (a), CryoSPARC homogeneous (b), Xmipp highres (c), and Relion 3D autorefine (d).

same concept applies to reprojections of a volume) gains Signal-to-Noise Ratio by averaging out the noise, then it starts "attracting" many other experimental images, even if they do not look like the reference. The reason is that the low contribution of the clean surrounding of the high SNR reference compensates for the mismatches of the reference itself. In 3D angular assignment this attraction would mean that a direction would attract particles from other directions, most likely nearby directions. This effect could well explain the differences reported in Fig. 2 of Sorzano et al. (2018). We have also observed this attraction problem in 3D classification, in which one of the classes attracts most of the particles, and a 2D classification shows that not all particles actually belong to that 3D class (results unpublished). The non-uniform reconstruction of CryoSPARC was specifically designed to avoid this problem of anisotropy, and Xmipp highres (Sorzano et al., 2018) seems to be also immune to it, probably due to its consideration of multiple objective functions.

Another possible reason for the harm caused by overabundant directions is that a proportion of these can be mistakenly assigned a projection direction far from their true position. Then, the information brought by the small number of non-overabundant projections (even in the best case that they are all correctly assigned) is swamped out by the flood of overabundant directions being incorrectly assigned.

In this technical note, we report on the 3D reconstruction of two more examples in which the angular distribution is radically different between different algorithms. In the first example, it seems that the anisotropy of the 3D angular assignment is purely caused by the angular assignment and 3D reconstruction algorithm. In the second case, it seems that the underlying angular distribution is really uneven, with an overabundance of top views. In this second case, Relion assigned all the images to almost a single direction making the 3D reconstruction impossible. CryoSPARC could not produce a high-resolution reconstruction of this dataset, neither, although it did not completely collapse the angular assignment to a single direction. We add a third example in which the cause of the elongation was not the angular assignment or the reconstruction algorithm but the sharpening step.

2. Results

We start with phantom data in which an uneven distribution of directions is simulated. We then move to three experimental cases.

2.1. Case 0: phantom data

To verify the effect of the overabundant directions, we selected the Erythromycin Resistant *Staphylococcus aureus* 50S ribosome in complex with erythromycin (EMDB entry: 10077 Halfon et al., 2019). We generated 14,000 projections at a pixel size of 1.07 Åand a box size of 300×300. 80% of the particles were top views within an angular cone of 20 degrees in diameter. We added noise to a SNR of about 1/2 and simulated a Contrast Transfer Function (CTF) (300 kV, 2.7 mm. of spherical aberration, 7% of amplitude contrast, and a defocus between 0.5 and 2.5 μm.), see Fig. 1 for some representative images. This should be an easy angular assignment case as there is not much noise. We used a low pass filtered version of the input volume at 12 Å. We aligned and reconstructed these images using CryoSparc non-uniform refinement, Relion 3D autorefine, and Xmipp highres. The average angular distance for the three algorithms were 2, 6, and degrees, respectively. The average shift error was 2 pixels for CryoSparc non-uniform refinement and 5 pixels for the other two. With an error smaller than 1 degree and 1 pixel, there were 530 images in CryoSparc, 2,754 images in Relion 3D autorefine and 7,603 in Xmipp highres. Interestingly, the lowest average error of CryoSparc does not correspond to a larger fraction of very accurately assigned particles. Actually, the resolution of the map reconstructed by CryoSparc was limited to 12.1Åand will not be furthered compared. The difference in the 3D reconstruction between the Relion and Xmipp was rather noticeable with strong elongations in the overloaded direction in the case of Relion 3D autorefine (see vertical lines in Fig. 1 bottom). The tilt angle distribution has been depleted from the 0–10° where the data was generated and assigned to an attracted tilt angle of 13–14° (which actually was not much represented in the original dataset; see Fig. 1). We used Relion reconstruction algorithm with the perfect angles or Relion 3D autorefine with a local refinement starting from the perfect angles, and they did not have any elongation, meaning that the elongation is induced by attraction to an incorrect orientation along the iterative process.

2.2. Case 1: a modified form of the myddosome

As the first example, we present a modified form of the myddosome whose biological details will be published elsewhere. 2,282 movies were recorded at a Titan Krios with a pixel size of 0.71 Å/pix. We estimated the Contrast Transfer Function (CTF) with CTFFind4 (Rohou et al., Nov 2015) and Xmipp (Sorzano et al., 2007) discarding those micrographs (132) with low-quality CTFs. 610 k coordinates were selected from the remaining micrographs using automatic picking tools (Abrishami et al., 2013). We cleaned in 2D the dataset using a combination of tools (Xmipp screen particles (Vargas et al., 2013), Relion 2D (Scheres et al., 2005) and Xmipp CL2D (Sorzano et al., 2010)) reducing this set to 341 k particles. We constructed an initial volume based on Xmipp tools (RANSAC (Vargas et al., 2014), reconstruct significant (Sorzano et al., 2015), and swarm consensus (Sorzano et al., 2018)). We then used Relion 3D classification (Scheres, 2012) to sort the particles into distinct 3D classes. In this manuscript, we show one of them, although the same problem was found in all of them. This class was formed by 77 k particles and, as can be seen in Suppl. Fig. 1a, it contained a wide range of different views. In Figs. 2a,b,c we show the reconstructions performed by CryoSPARC non-uniform reconstruction, CryoSPARC homogeneous refinement, and Xmipp highres, respectively. These reconstructions did not have a significant elongation of the structure. However, the 3D reconstruction performed by Relion 3D autorefine showed a severe preferred orientation problem (see Fig. 2d for the reconstruction and Suppl. Fig. 1b for the angular distribution). The median local resolution

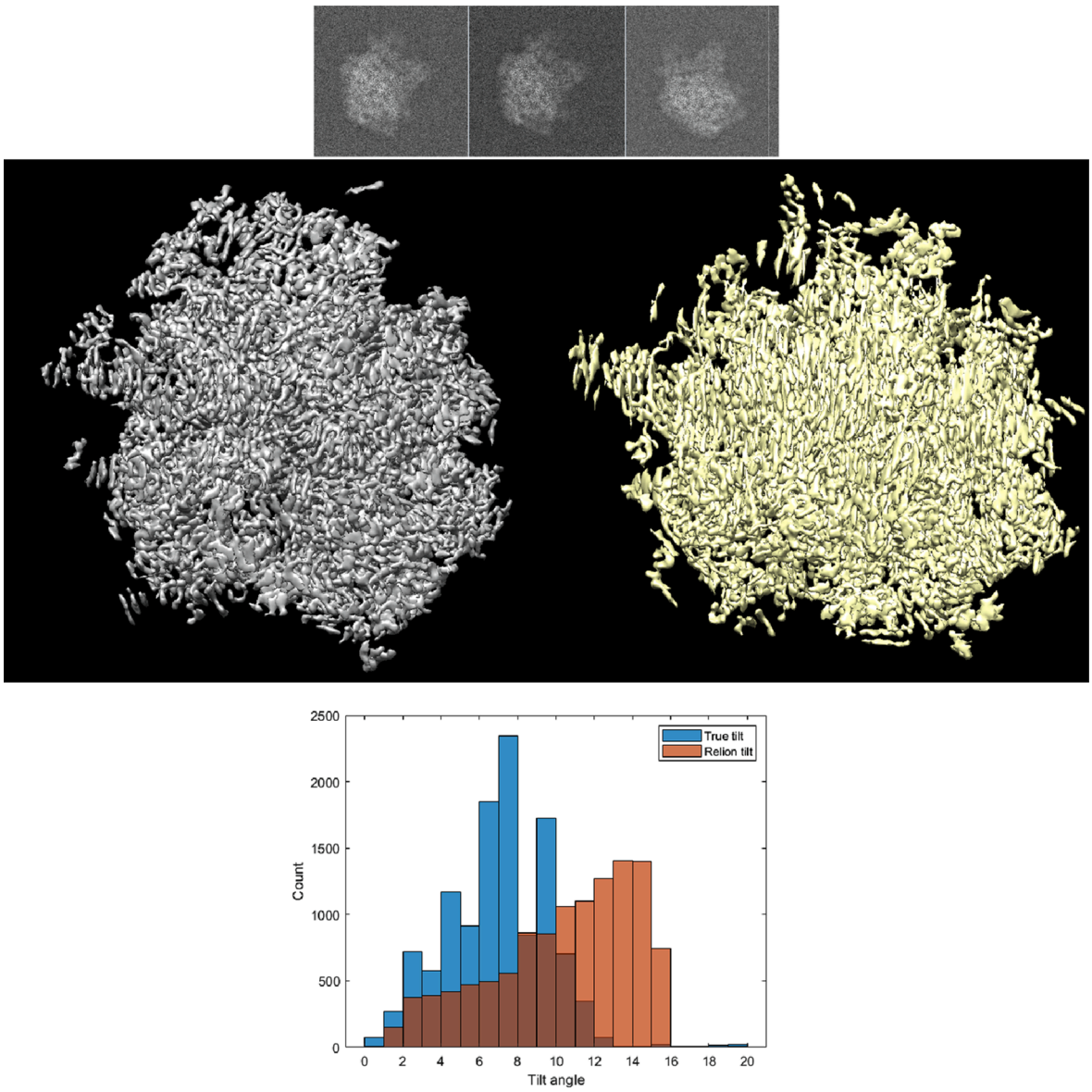

Fig. 1. Top: Example of simulated images. Middle: Reconstructed volume by Xmipp highres (left) and Relion 3D autorefine (right). Bottom: True tilt angle distribution and the one assigned by Relion.

measured by deepRes (Ramírez-Aportela et al., 2019) was 5.71 Å(for CryoSPARC non-uniform), 5.29 Å(for Relion autorefine), and 5.12 Å(for Xmipp highres). We note that there is no sharpening operation involved in any of the three results.

2.3. Case 1: tetrameric photosystem I

For the second example, we show a tetrameric photosystem I (PSI) whose biological details will also be published elsewhere. 4,845 movies were recorded at a Titan Krios with a pixel size of 1.11 Å/pix. We followed an image processing pipeline similar to the one described in the previous example. 372 micrographs were dropped due to CTF considerations. We picked 336 k coordinates that after 2D class analysis finished in 91 k particles. In this case, the 2D classes showed a very biased angular distribution with top views being more abundant than the rest of the views (see Suppl. Fig. 2). We constructed the initial volume using the same tools as above. Using Xmipp highres, the set of particles was further reduced to 66 k particles, and the 3D reconstruction had a resolution of 3.8Å(see Suppl. Fig. 2). The same particles reconstructed with CryoSPARC homogeneous and non-uniform reconstructions yielded a volume of only 9.3Å, and with Relion 3D autorefine 8.8Å. The reconstruction of this structure can be seen in Fig. 3, and despite the seemingly medium resolution of CryoSPARC and Relion auto-refine, their reconstructed structural features are clearly incorrect since both programs place electron density in the central, interior cavity. As shown in the top image of Fig. 3, this region is empty and devoid of any regular electron-dense material such as lipids, pigments, or protein subunits.

2.4. Case 3: human epidermal growth factor receptor 2

Our last example shows the results of the human epidermal growth factor receptor 2 (HER2) acquired in a collaborative project. 3,138 micrographs at a pixel size of 0.42 Å/pixel were acquired in a Titan Krios with a K3 camera in superresolution mode. 1.2 M coordinates were identified that resulted, after 2D and 3D classification, in 270 k particles. These particles had a strong preferential orientation, as shown in Suppl. Fig. 3. CryoSPARC homogeneous and non-uniform reconstructions had a slight elongation along the overloaded direction. However, this elongation was largely exaggerated by CryoSPARC local sharpening (see

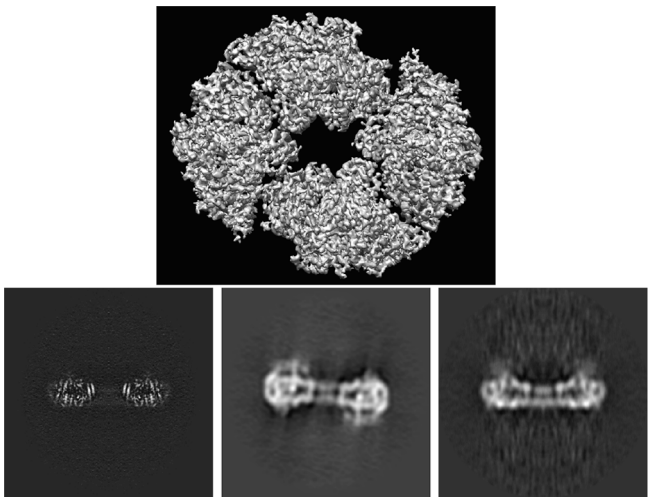

Fig. 3. Top: Reconstruction of a tetrameric photosystem I by Xmipp highres. Bottom: Central slice of the reconstruction by Xmipp highres (left), CryoSPARC non-uniform reconstruction (middle), and Relion 3D autorefine (right).

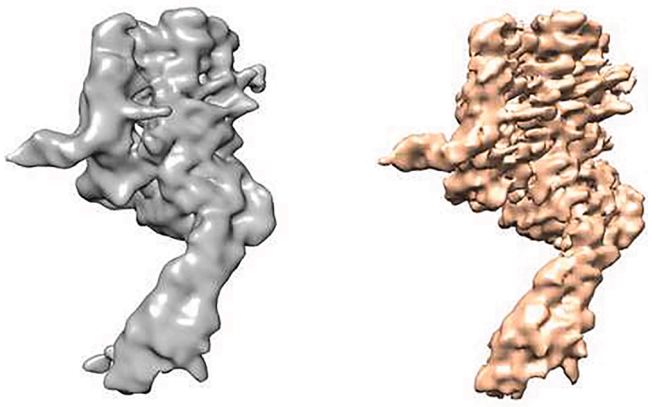

Fig. 4. Side view of the HER2 protein after CryoSPARC non-uniform reconstruction (left) and CryoSPARC local sharpening (right).

Fig. 4; the resolution reported by CryoSPARC for this structure was 4.1Å). Other deblurring algorithms like localDeblur (Ramírez-Aportela et al., 2019) also resulted in pronounced elongations. Note that the objective of this example is to make the practitioner aware that normally well-behaved algorithms (like CryoSPARC local sharpening or localDeblur) may be responsible for exaggerating directional problems. That is, there is still room for improvement in the algorithmic handling of anisotropic SNRs.

3. Discussion and conclusions

Problems with overabundant directions have recurrently appeared in EM image processing (see Sorzano et al., 2001 and the references therein). The problem reported in Sorzano et al. (2001) was related to the reconstruction algorithm and not to the angular assignment. Volume elongations along the overabundant directions were introduced by an incorrect choice of the reconstruction algorithm parameters. Current reconstruction algorithms based on Fourier gridding (Penczek et al., 2004; Scheres, 2012; Abrishami et al., 2015) have fewer parameters and seem to be much more robust to the presence of overabundant directions thanks to the explicit evaluation of the local density of measurements in the 3D Fourier space.

The problem reported in this technical note is more fundamental and seems to be related to the nature of the distance used to evaluate the similarity between pairs of images. Although the mathematics of Relion and CryoSPARC seem to be totally different to the ones of Xmipp highres, they all share two fundamental characteristics that make them similar in nature: 1) a multiresolution approach in which the problem is solved first in low resolution, and new information is added as the internal consistency of the reconstruction increases; 2) the overall structure of a weighted 3D reconstruction in which particles enter in the 3D reconstruction, at multiple places in the case of Relion, with different weights.

We believe that the differences in the multiresolution implementation (in Relion, it is implemented by low pass filtering while in Xmipp highres, it is implemented by downsampling) cannot explain the different behaviors of the two algorithms (note that both strategies are fundamentally the same except for the falloff of the filter at the transition frequency band) and that the main difference is in the different weighting schemes. In the first iterations of Relion, particles can occupy many different orientations with a weight that is given by a weighted sum of squares of the residual between the experimental and the reprojected image. A careful analysis of this sum of squares reveals that differences are relatively small (even in the last iterations) among a large subset of possible orientations. This scheme allows the possibility that in the first iterations, many particles contribute to a particular projection direction, increasing its SNR by reducing the noise background around the reprojection. Once some directions have increased their SNR, they may enter into a positive feedback loop due to the attraction problem described in Sorzano et al. (2010). In Xmipp highres, a projection can occupy only one position in the projection sphere (although the implementation of the algorithm allows a projection occupying several locations, it is not recommended more than one), and the weight is determined from the statistical significance of two similarity measures (cross-correlation and IMED Li and Lu, 2009) when an experimental image is compared to the whole set of volume reprojections, and by the statistical significance when a reprojection is compared to the whole set of experimental images. There are two key advantages in this approach: 1) several similarity measures determine the weight (additionally, IMED is slightly more sensitive to small differences in highly matching pairs of images, see Fig. 2 in Sorzano et al. (2015)) avoiding overfitting problems because the local minima of one of the measures is not necessarily a local minimum of the other; 2) the weight is not calculated solely on the "desire" of an experimental image to find its place in the projection sphere, but also on the quality of this fitting when compared to the whole set of experimental images. This is captured by the significance of these similarity measures when a single reprojection is compared to the whole experimental set. This second feature makes that a poorly matching experimental image is assigned a low weight in its assigned projection direction, even if this projection direction is the best match for this experimental particle.

A second possible explanation, probably coexisting with the one above, is that if the same particle is allowed to occupy several projection directions, then the incorrectly assigned set of orientations may swamp the information brought by the rest of the particles, resulting in a loss of resolution, and ultimately of useful information.

Another strategy followed by CryoSPARC non-uniform reconstruction, Xmipp highres, and lately suggested by Lafter (Ramlaul et al., 2019) is removing noise anchors that could drive the angular assignment. CryoSPARC non-uniform reconstruction follows this strategy using an anisotropic filter and Xmipp highres and Lafter by analyzing the gold-standard strategy's two halves and dampening those features that do not outstand above the level of noise.

We have also shown that the sharpening algorithm is not immune to this anisotropic SNR and that it may result in an overdampening in Fourier space of some directions (the overloaded ones). This overdampening because this direction has a lower SNR than its perpendicular counterparts causes an elongation in real space along the overabundant direction.

Some EM practitioners in the 90's proposed to drop images from the

overabundant direction for homogenizing the angular distribution. A better solution at that time was algorithmic so that no experimental information had to be discarded. At present, some experiments are currently being fully dropped because of the structural artifacts encountered with these uneven angular distributions. Again, an algorithmic resort may save the situation. Obviously, angular assignment, reconstruction, and sharpening algorithms cannot compensate for the lack of measured directions, but they should not penalize the abundance of measurements in other directions.

As a final remark, we would like to emphasize that the examples given in this article are not meant to diminish any particular algorithm's importance. On the contrary, they are meant to highlight that algorithms themselves, all of them and normally well behaved, play a role in interpreting the data and that reliable biological information is gained only if different algorithms confirm the same results. But, this is the subject of a different manuscript (Sorzano et al., 2020). The purpose of this manuscript is not to highlight the robustness of any particular algorithm as opposed to the others or make a thorough statistical analysis of the proportion of cases in which one, two, or three algorithms succeed or fail in the presence of uneven angular distributions. It is to highlight the fact that there are situations in which the algorithm itself cannot handle an experimental uneven distribution or may even induce this uneven distribution.

Declaration of Competing Interest

The authors declare that they have no known competing financial interests or personal relationships that could have appeared to influence the work reported in this paper.

Acknowledgements

We acknowledge support from "la Caixa" Foundation (Fellowship LCF/BQ/DI18/11660021. This project has received funding from the European Union's Horizon 2020 research and innovation program under the Marie Sklodowska-Curie grant agreement No. 713673. We also thank the financial support from the Spanish Ministry of Economy and Competitiveness through Grants BIO2016-76400-R(AEI/FEDER, UE) and SEV 2017-0712, the "Comunidad Autónoma de Madrid" through Grant: S2017/BMD-3817, Instituto de Salud Carlos III, PT17/0009/0010 (ISCIII-SGEFI/ERDF), European Union (EU) and Horizon 2020 through grants: CORBEL (INFRADEV-1-2014-1, Proposal: 654248), INSTRUCT-ULTRA (INFRADEV-03-2016-2017, Proposal: 731005), EOSC Life (INFRAEOSC-04-2018, Proposal: 824087), HighResCells (ERC-2018-SyG, Proposal: 810057), IMpaCT (WIDESPREAD-03-2018 – Proposal: 857203), EOSC-Synergy (EINFRA-EOSC-5, Proposal: 857647), and iNEXT-Discovery (Proposal: 871037). The authors acknowledge the support and the use of resources of Instruct, a Landmark ESFRI project.

Appendix A. Supplementary data

Supplementary data associated with this article can be found, in the online version, athttps://doi.org/10.1016/j.jsb.2020.107695.

References

Abrishami, V., Bilbao-Castro, J.R., Vargas, J., Marabini, R., Carazo, J.M., Sorzano, C.O.S., 2015. A fast iterative convolution weighting approach for gridding-based direct fourier three-dimensional reconstruction with correction for the contrast transfer function. Ultramicroscopy 157, 79–87.

Abrishami, V., Zaldívar-Peraza, A., de la Rosa-Trevín, J.M., Vargas, J., Otón, J., Marabini, R., Shkolnisky, Y., Carazo, J.M., Sorzano, C.O.S., 2013. A pattern matching approach to the automatic selection of particles from low-contrast electron micrographs. Bioinformatics 29 (19), 2460–2468.

Boisset, N., Penczek, P., Taveau, J.C., You, V., de Haas, F., Lamy, J., 1998. Overabundant single-particle electron microscope views induce a three-dimensional reconstruction artifact. Ultramicroscopy 74, 201–207.

D'Imprima, E., Floris, D., Joppe, M., Sanchez, R., Grininger, M., Kuhlbrandt, W., 2019. Protein denaturation at the air-water interface and how to prevent it. eLife 8.

Halfon, Y., Matzov, D., Eyal, Z., Bashan, A., Zimmerman, E., Kjeldgaard, J., Ingmer, H., Yonath, A., 2019. Exit tunnel modulation as resistance mechanism of s. aureus erythromycin resistant mutant. Scientific Rep. 9 (1), 1–8.

Li, J., Lu, B.L., 2009. An adaptive image euclidean distance. Pattern Recogn. 42, 349–357.

Naydenova, K., Russo, C.J., 2017. Measuring the effects of particle orientation to improve the efficiency of electron cryomicroscopy. Nat. Commun. 8, 629.

Noble, A.J., Dandey, V.P., Wei, H., Brasch, J., Chase, J., Acharya, P., Tan, Y.Z., Zhang, Z., Kim, L.Y., Scapin, G., Rapp, M., Eng, E.T., Rice, W.J., Cheng, A., Negro, C.J., Shapiro, L., Kwong, P.D., Jeruzalmi, D., des Georges, A., Potter, C.S., Carragher, B., 2018. Routine single particle cryoEM sample and grid characterization by tomography. eLife 7, e34257.

Noble, A.J., Wei, H., Dandey, V.P., Zhang, Z., Tan, Y.Z., Potter, C.S., Carragher, B., 2018. Reducing effects of particle adsorption to the air-water interface in cryo-EM. Nat. Methods 15, 793–795.

Penczek, P., 2002. Three-dimensional spectral signal-to-noise ratio for a class of reconstruction algorithms. J. Struct. Biol. 138, 34–46.

Penczek, P., Renka, R., Schomberg, H., 2004. Gridding-based direct fourier inversion of the three-dimensional ray transform. J. Opt. Soc. Am. A 21, 499–509.

Ramírez-Aportela, E., Mota, J., Conesa, P., Carazo, J.M., Sorzano, C.O.S., 2019. Deepres: a new deep-learning- and aspect-based local resolution method for electron-microscopy maps. IUCRj 6, 1054–1063.

Ramírez-Aportela, E., Vilas, J.L., Glukhova, A., Melero, R., Conesa, P., Martínez, M., Maluenda, D., Mota, J., Jiménez, A., Vargas, J., Marabini, R., Sexton, P.M., Carazo, J.M., Sorzano, C.O.S., 2019. Automatic local resolution-based sharpening of cryo-EM maps. Bioinformatics 36, 765–772.

Ramlaul, K., Palmer, C.M., Aylett, C.H.S., 2019. A local agreement filtering algorithm for transmission em reconstructions. J. Struct. Biol. 205, 30–40.

Rohou, A., Grigorieff, N., 2015. Ctffind4: fast and accurate defocus estimation from electron micrographs. J. Struct. Biol. 192 (2), 216–221.

Russo, C.J., Passmore, L.A., 2014. Electron microscopy. ultrastable gold substrates for electron cryomicroscopy. Science 346 (6215), 1377–1380.

Scheres, S.H.W., 2012. A Bayesian view on cryo-EM structure determination. J. Mol. Biol. 415, 406–418.

Scheres, S.H.W., 2012. Relion: implementation of a bayesian approach to cryo-EM structure determination. J. Struct. Biol. 180, 519–530.

Scheres, S.H.W., Valle, M., Núñez, R., Sorzano, C.O.S., Marabini, R., Herman, G.T., Carazo, J.M., 2005. Maximum-likelihood multi-reference refinement for electron microscopy images. J. Mol. Biol. 348, 139–149.

Sorzano, C.O.S., Bilbao-Castro, J.R., Shkolnisky, Y., Alcorlo, M., Melero, R., Caffarena-Fernández, G., Li, M., Xu, G., Marabini, R., Carazo, J.M., 2010. A clustering approach to multireference alignment of single-particle projections in electron microscopy. J. Struct. Biol. 171, 197–206.

Sorzano, C.O.S., Jiménez-Moreno, A., Maluenda, D., Martínez, M., Ramírez-Aportela, E., Melero, R., Cuervo, A., Conesa, J., Filipovic, J., Conesa, P., del Caño, L., Fonseca, Y. C., Jiménez-de la Morena, J., Losana, P., Sánchez-García, R., Strelak, D., Fernández-Giménez, E., de Isidro, F., Herreros, D., Vilas, J.L., Marabini, R., Carazo, J.M., 2020. On bias, variance, overfitting, gold standard and consensus in single particle analysis by cryo-electron microscopy. Curr. Res. Struct. Biol. (under review).

Sorzano, C.O.S., Jonic, S., Núñez Ramírez, R., Boisset, N., Carazo, J.M., 2007. Fast, robust and accurate determination of transmission electron microscopy contrast transfer function. J. Struct. Biol. 160, 249–262.

Sorzano, C.O.S., Marabini, R., Boisset, N., Rietzel, E., Schröder, R., Herman, G.T., Carazo, J.M., 2001. The effect of overabundant projection directions on 3D reconstruction algorithms. J. Struct. Biol. 133, 108–118.

Sorzano, C.O.S., Vargas, J., de la Rosa-Trevin, J.M., Jimenez, A., Maluenda, D., Melero, R., Martinez, M., Ramirez-Aportela, E., Conesa, P., Vilas, J.L., Marabini, R., Carazo, J.M., 2018. A new algorithm for high-resolution reconstruction of single particles by electron microscopy. J. Struct. Biol. 204, 329–337.

Sorzano, C.O.S., Vargas, J., de la Rosa-Trevín, J.M., Otón, J., Álvarez-Cabrera, A.L., Abrishami, V., Sesmero, E., Marabini, R., Carazo, J.M., 2015. A statistical approach to the initial volume problem in single particle analysis by electron microscopy. J. Struct. Biol. 189, 213–219.

Sorzano, C.O.S., Vargas, J., Vilas, J.L., Jiménez-Moreno, A., Mota, J., Majtner, T., Maluenda, D., Martínez, M., Sánchez-García, R., Segura, J., Otón, J., Melero, R., del Cano, L., Conesa, P., Gómez-Blanco, J., Rancel, Y., Marabini, R., Carazo, J.M., 2018. Swarm optimization as a consensus technique for electron microscopy initial volume. Appl. Anal. Optim. 2, 299–313.

Turonova, B., Marsalek, L., Slusallek, P., 2016. On geometric artifacts in cryo electron tomography. Ultramicroscopy 163, 48–61.

Unser, M., Sorzano, C.O.S., Thévenaz, P., Jonic, S., El-Bez, C., De Carlo, S., Conway, J., Trus, B.L., 2005. Spectral Signal-to-Noise Ratio and resolution assessment of 3D reconstructions. J. Struct. Biol. 149, 243–255.

Vargas, J., Abrishami, V., Marabini, R., de la Rosa-Trevín, J.M., Zaldivar, A., Carazo, J. M., Sorzano, C.O.S., 2013. Particle quality assessment and sorting for automatic and semiautomatic particle-picking techniques. J. Struct. Biol. 183, 342–353.

Vargas, J., Álvarez-Cabrera, A.L., Marabini, R., Carazo, J.M., Sorzano, C.O.S., 2014. Efficient initial volume determination from electron microscopy images of single particles. Bioinformatics 30, 2891–2898.

Wei, H., Dandey, V.P., Zhang, Z., Raczkowski, A., Rice, W.J., Carragher, B., Potter, C.S., 2018. Optimizing "self-wicking" nanowire grids. J. Struct. Biol. 202, 170–174.

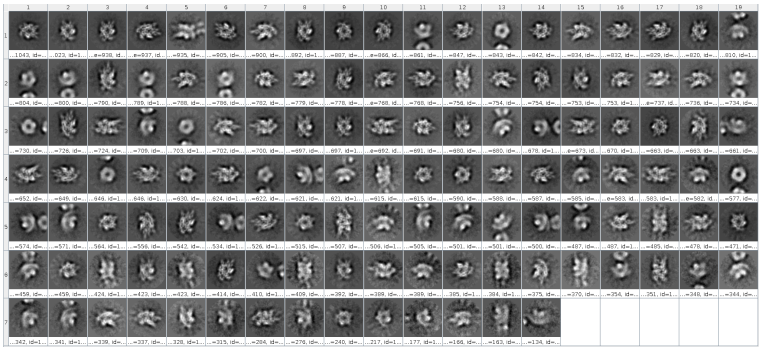

(a) Classes 2D from one of the 3D classes identified by Relion 3D Classification

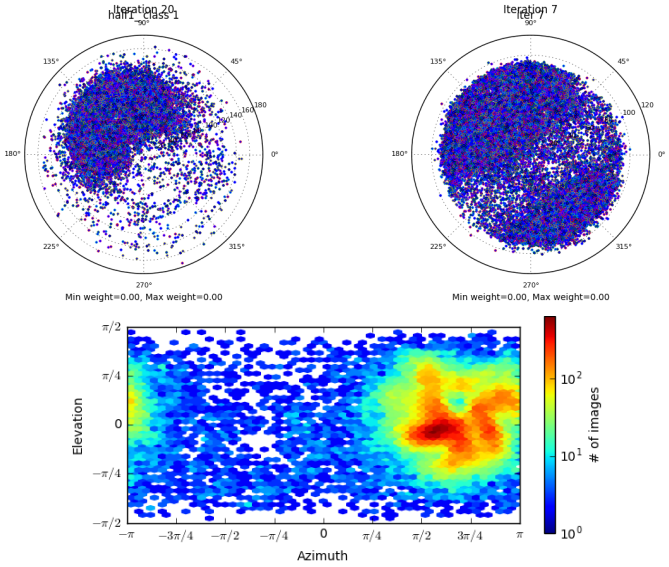

(b) Angular distribution as calculated by Relion 3D autorefine (top left), Xmipp high-res (top right) and CryoSPARC non-homogeneous (bottom).

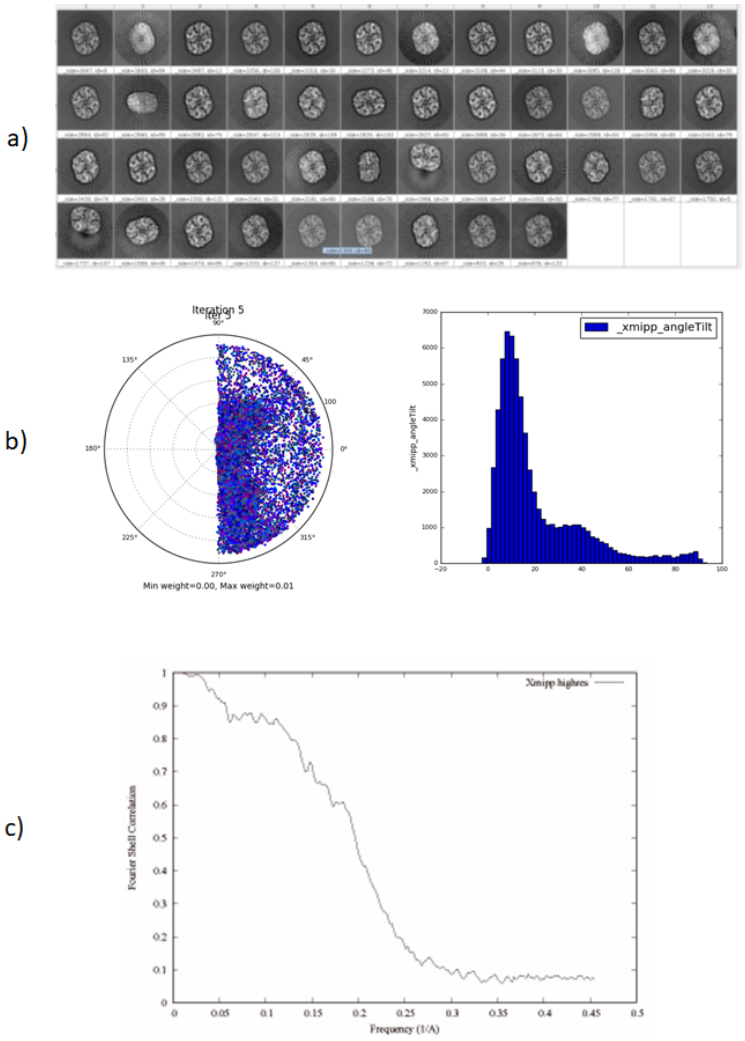

Figure 2: a) 2D Classes of tetrameric PSI. b) Angular distribution as calculated by Xmipp highres (left) and the histogram of the tilt angle (right) showing that most of the particles corresponded to top views. c) Gold standard FSC of the 3D reconstruction performed by Xmipp highres.

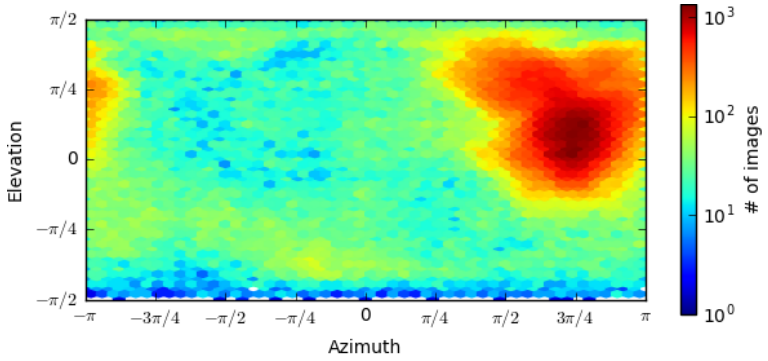

Figure 3: Angular distribution of the HER2 dataset calculated by CryoSPARC non-uniform 3D reconstruction algorithm.